Phase behaviour of polarizable colloidal hard rods in an external electric field: A simulation study

Thomas Troppenz, Laura Filion, René van Roij, and Marjolein Dijkstra

Citation: The Journal of Chemical Physics **141**, 154903 (2014); doi: 10.1063/1.4897562
View online: http://dx.doi.org/10.1063/1.4897562
View Table of Contents: http://scitation.aip.org/content/aip/journal/jcp/141/15?ver=pdfcov
Published by the AIP Publishing

Phase behaviour of polarizable colloidal hard rods in an external electric field: A simulation study

Thomas Troppenz,[1] Laura Filion,[2] René van Roij,[1] and Marjolein Dijkstra[2]
[1]*Institute for Theoretical Physics, Utrecht University, Leuvenlaan 4, 3584 CE Utrecht, The Netherlands*
[2]*Debye Institute for Nanomaterials Science, Utrecht University, Princetonplein 5, 3584 CC Utrecht, The Netherlands*

(Received 15 April 2014; accepted 30 September 2014; published online 20 October 2014)

We present a double-charge model for the interaction between parallel polarizable hard spherocylinders subject to an external electric field. Using Monte Carlo simulations and free-energy calculations, we predict the phase behaviour for this model as a function of the density and electric field strength, at a fixed length-to-diameter ratio $L/D = 5$. The resulting phase diagram contains, in addition to the well-known nematic, smectic A, ABC crystal, and columnar phases, a smectic C phase, and a low temperature crystal X phase. We also find a string fluid at low densities and field strengths, resembling results found for dipolar spheres. © *2014 AIP Publishing LLC*. [http://dx.doi.org/10.1063/1.4897562]

I. INTRODUCTION

Polarizable colloidal spheres with a dielectric constant mismatch with the surrounding solvent acquire a dipole moment in an external electric field. The resulting dipolar interactions between the colloids lead to the formation of string-like clusters where the dipoles are aligned head-to-toe.[1–3] As a result, the rheological properties of these suspensions can be tuned by the electric field. Therefore, these so-called electro-rheological fluids have potential use in industrial applications such as hydraulic valves, brake fluids, and bullet-proof vests.

To a first-order approximation, the phase behaviour of these suspensions is well-described by a dipolar interaction between point dipoles, which are aligned with the applied field and located in the center of each colloidal sphere. The phase diagram in this approximation is well studied and displays a string fluid at low density and high field strength, a face-centered cubic crystal at high density and vanishing field strength, a hexagonal close-packed crystal at high density and moderate to high field strength, as well as a less dense body-centered tetragonal crystal phase at intermediate density and high field strength.[1,2] Additionally, a body-centered orthogonal crystal phase is observed for intermediate field strength and density in the case of soft repulsive spheres.[1–3] The phase behaviour of anisotropic colloidal particles, such as rods,[4–6] dumbbells,[7–9] snowman particles,[10,11] and bowls,[12,13] has received significantly less attention, even though great progress has been made in the synthesis of such particles in recent times (see, e.g., Ref. 14). Furthermore, it is well known that electric fields can be used to control not only the relative position,[1,2] but also the orientation of such anisotropic particles.[7,8,15–18] In the present paper, we focus on the phase behaviour of rod-like colloidal particles in the presence of an external electric field. The aim of this paper is the construction of a phase diagram corresponding to experiments recently carried out on systems of micron-sized silica rods.[19]

From experiments[15,19] and theoretical calculations,[17] we know that polarizable rods align their symmetry axis in the direction of a strong external electric field. Here, we assume that this alignment with the field is perfect, i.e., that all spherocylinders are aligned in the direction of the field. This assumption can be largely justified as we expect nematic ordering of the rods for (i) sufficiently high packing fractions[20] and (ii) sufficiently high field strength.[17] In particular, we consider a system of hard parallel polarizable spherocylinders subject to an external electric field. The spherocylinders are modeled by a cylindrical part of length L and diameter D, with both ends capped by a hemisphere. We show that the dipolar interaction between a pair of such spherocylinders is well approximated by the interaction of two opposite charges near the ends of the spherocylinder. We use Monte Carlo (MC) simulations and free-energy calculations to determine the phase diagram of this model in the plane spanned by the packing fraction of spherocylinders and the strength of their mutual dipolar interactions. We also present the equation of state for different interaction strengths and discuss the possibility of chain formation.

II. THE MODEL

In order to describe the phase behaviour of polarizable colloidal rods in an external electric field, we require a model that offers a compromise between accuracy and simulation speed. To this end, we model the particles by hard, parallel, polarizable spherocylinders with aspect ratio $L/D = 5$. The polarization is modeled by placing two opposite point charges $\pm q$ in the hemispherical end caps of the spherocylinders, displaced a distance δ_z from the center of the hemispheres, see Fig. 1. In this approximation, the potential between two parallel spherocylinders separated by a distance vector $\mathbf{r}$ is given by

$$\beta V(\mathbf{r}) = \begin{cases} \beta V_{dc}(\mathbf{r}), & \text{if the rods do not overlap} \\ \infty, & \text{if the rods overlap} \end{cases}, \quad (1)$$

where $\beta = 1/k_B T$, with k_B the Boltzmann constant and T the temperature. The interaction between two rods which do not

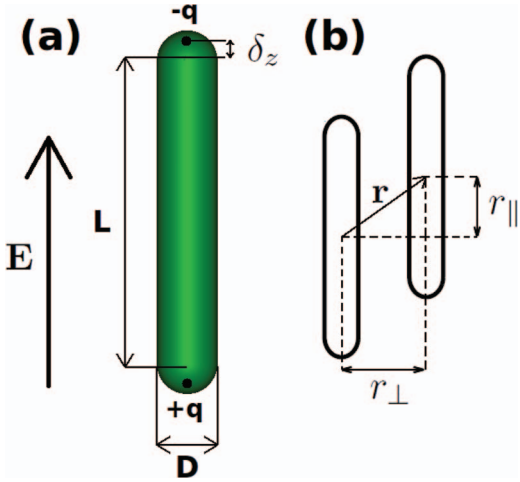

FIG. 1. (a) Schematic picture of the double-charge model for spherocylinders of cylinder length L and diameter D. The interaction between parallel polarizable spherocylinders subject to an external electric field is approximated by the interaction between pairs of point charges with charge $\pm q$ in each spherocylinder which are displaced by a distance $\delta_z \approx 0.276D$ from the centers of their hemispherical end caps. (b) Sketch of two parallel polarizable spherocylinders. Their relative distance $\mathbf{r}$ has a component $r_\parallel$ parallel to the electric field and a perpendicular component $r_\perp$.

overlap is given by the double-charge potential

$$\beta V_{dc}(r_\parallel, r_\perp) = \gamma \left(\frac{2D}{r} - \frac{D}{\sqrt{r_\perp^2 + (r_\parallel + L + 2\delta_z)^2}} - \frac{D}{\sqrt{r_\perp^2 + (r_\parallel - L - 2\delta_z)^2}} \right), \quad (2)$$

where $r_\perp$ and $r_\parallel$ denote the distances between the centers of the spherocylinders in the direction perpendicular and parallel to the field, and r is the magnitude of $\mathbf{r}$, see Figure 1(b). The proportionality constant γ is given by

$$\gamma = \frac{\beta q^2}{4\pi \epsilon_{\text{sol}} D}, \quad (3)$$

where ϵ_{sol} is the dielectric constant of the solvent.

In order to relate the proportionality constant γ to the applied electric field E, we approximate the rod as a uniformly polarized dielectric with dielectric constant ϵ_{rod}. Within this approximation, the dipole moment of the rod is given by

$$p_{\text{rod}} = \alpha E, \quad (4)$$

where α is given by the Clausius–Mossotti relation

$$\alpha = 3 v_{\text{rod}} \epsilon_{\text{sol}} \left(\frac{\epsilon_{\text{rod}} - \epsilon_{\text{sol}}}{\epsilon_{\text{rod}} + 2\epsilon_{\text{sol}}} \right), \quad (5)$$

with v_{rod} the volume of the rod. This approximation ignores variations in the polarization strength and direction inside the rod, as well as any polarization due to the electric field resulting from neighboring rods. Note that the later assumption is valid when α is small.[21]

In the double charge model, the dipole moment is given by

$$p_{\text{rod}}^{\text{dc}} = q(L + 2\delta_z). \quad (6)$$

Equating the dipole moments $p_{\text{rod}} = p_{\text{rod}}^{\text{dc}}$, we obtain

$$q = \left(\frac{\alpha}{L + 2\delta_z} \right) E. \quad (7)$$

To determine the exact position of the charges inside the rods, i.e., δ_z, we compare the potential energy landscape between two rods within the double charge approximation (V_{dc}) to that of two rods within a permanent dipole model (V_{pd}). In this permanent dipole model, we model each rod as $N_d \approx 6100$ point dipoles arranged on a simple cubic lattice of lattice constant a in the shape of a spherocylinder. The number of point dipoles was determined by decreasing the lattice spacing until we observed convergence of the interparticle interaction in several configurations, and then choosing a slightly smaller value of the lattice spacing. We relate the strength of the small dipoles in the permanent dipole model to the strength of the charges in the double-charge model by demanding that the dipole moment p_{rod} equals the total dipole moment of the small dipoles. We introduce

$$\delta v(r_\perp, r_\parallel, \delta_z) = \frac{|V_{\text{pd}}(r_\perp, r_\parallel) - V_{\text{dc}}(r_\perp, r_\parallel, \delta_z)|}{|V_{\text{dc}}(0, L + D, \delta_z)|}, \quad (8)$$

as a measure of the relative difference in interaction strength between the double-charge model and the permanent dipole model for three typical configurations. A plot of $\delta v(r_\perp, r_\parallel, \delta_z)$ as a function of δ_z is depicted in Fig. 2. We find good agreement between the two models when $\delta_z \approx 0.276D$.

Figure 3 shows a comparison between V_{dc} and V_{pd} as a function of the relative position of two rods for $\delta_z = 0.276D$. As can be seen from Fig. 3, the relative difference between the two models is typically less than a few percent demonstrating that the double charge model with $\delta_z = 0.276D$ yields a good approximation for the potential between the rods. Note that the "ideal" value for δ_z varies only slightly depending on the lattice type and lattice spacing used in the permanent dipole approximation.

In the remainder of this paper, we study the phase behaviour of spherocylinders within the double charge model with $\delta_z = 0.276D$ using Monte Carlo simulations together with free-energy calculations. In the simulations, we

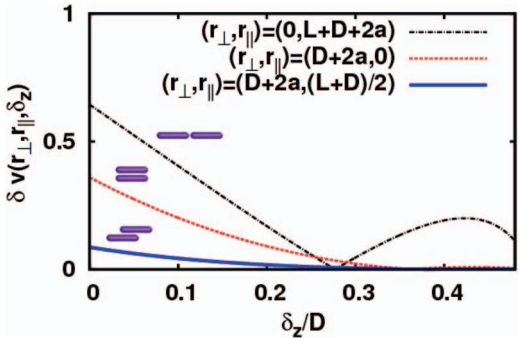

FIG. 2. Plot of $\delta v(r_\perp, r_\parallel, \delta_z)$, the absolute value of the relative difference between the double-charge potential V_{dc} and the reference potential V_{pd} between two hard parallel spherocylinders for three choices of $r_\perp$ and $r_\parallel$ as a function of δ_z. Note that a is the lattice constant in the permanent dipole model.

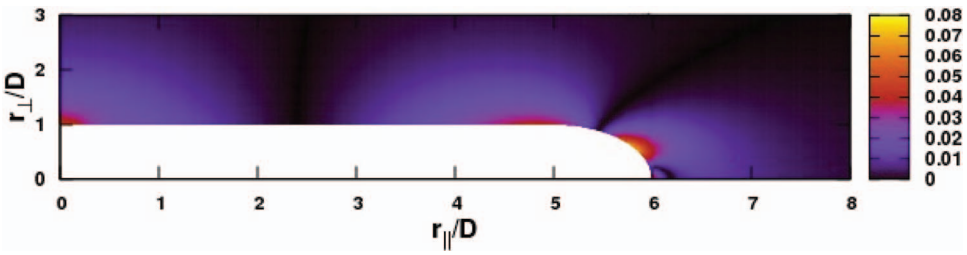

FIG. 3. Plot of $\delta v(r_\perp, r_\parallel, \delta_z = 0.276D)$ as defined in Eq. (8) for two parallel spherocylinders with $L/D = 5$ as a function of their relative distance $(r_\perp, r_\parallel)$ showing deviations between the double-charge model and the permanent dipole model of the order of a few percent at most.

implement the long-ranged interactions between the point charges using Ewald summations (see Ref. 22 for details).

III. PHASE DIAGRAM

The main objective of this paper is to establish the phase diagram of parallel hard polarizable rods in an external electric field. To this end, we first identify possible stable phases. Second, using thermodynamic integration we calculate the Helmholtz free energies of these phases. Finally, we use common tangent constructions to determine the coexistence regions, and draw the resulting phase diagram.

A. Candidate phases

The phase diagram for parallel hard rods has been examined in detail previously using computer simulations.[23] The resulting phase diagram consists of a stable nematic, a smectic *A*, and two crystalline phases with *AAA* and *ABC* stacking of hexagonal layers. Hence, we identify these four phases as candidate phases for our system. Note that the *AAA* phase is essentially a crystalline version of the smectic *A* phase where the layers are hexagonally ordered, and the *ABC* phase is the rod equivalent of the face-centered-cubic crystal phase for spheres.

Previous studies of polarizable rods of length $L/D = 2$ in an external electric field identified a distinct low-temperature phase called K_2 where the particles were aligned into columns with the columns hexagonally arranged and staggered in height from their neighbours by an offset of $(L + D)/3$ resulting in a crystalline phase with C_3 symmetry.[24] For our system, *NPT* Monte Carlo simulations showed that this structure melted for all investigated pressures P and temperatures T. Hence, this structure is clearly not stable for the present set of parameters. Nonetheless, it seems likely that crystal structures consisting of staggered columns of rods aligned along the direction of the external field, similar to the K_2 crystal structure, will be stable at low temperatures (high field strength) in our system. The optimal choices for the offsets of each column along the field direction may depend on the aspect ratio of the rods. In order to find candidate crystal structures for $L/D = 5$, we therefore investigated a range of these columnar crystal structures, and determined which choices were at least metastable in *NPT* Monte Carlo simulations. This search resulted in three candidate crystal structures (see Ref. 22 for details). We selected the phase with the lowest free energy as a candidate phase. A description of how the free energy was calculated is presented in Sec. III B. For the remainder of this paper we will refer to this structure as crystal *X*. Cartoons of the *X* structure, as well as the other phases found to be stable in the phase diagram, can be seen in Fig. 4. We note here that our study was not exhaustive, and it is possible that we missed stable crystal structures in our investigations. However, the structure we find with the lowest free energy has significant similarities with the crystals seen experimentally in this system.[19] Moreover, the unit vectors of crystal *X*,

$$\begin{aligned} \mathbf{k}_1^X &= (D, 0, D), \\ \mathbf{k}_2^X &= (-D/2, \sqrt{3}D/2, -2D), \\ \mathbf{k}_3^X &= (-D/2, -\sqrt{3}D/2, D), \end{aligned} \tag{9}$$

build up not only the K_2 crystal for $L/D = 2$ but also the *X* crystal for $L/D = 5$. The two structures *X* and K_2 are therefore closely related.

B. Free-energy calculations

In the following, we describe the details of the free-energy calculations for the individual phases of perfectly aligned rods examined in this study.

1. Free energy of the nematic phase

We determine the free energy per particle of the nematic phase, f by integrating the measured equation of state $P(\rho)$ from the low density limit $\rho \to 0$, where $\rho = N/V$ is the density. In this limit, the free energy reduces to that of the ideal gas,[25] and at finite ρ we have

$$\beta f(\rho) = \beta f_{id}(\rho) + \int_0^\rho d\rho' \left(\frac{\beta P(\rho') - \rho'}{\rho'^2} \right), \tag{10}$$

with f_{id} the free energy per particle of a noninteracting three dimensional gas of a finite number of rods in the double-charge model,

$$\begin{aligned} \beta f_{id}(\rho) \simeq \log \rho \Lambda^3 - 1 + \frac{1}{2N} \log 2\pi N \\ - \gamma D \frac{1}{L + 2\delta_z}, \end{aligned} \tag{11}$$

with Λ the thermal de Broglie wavelength of a rod. Note that the second last term corrects for the finite system size up to order $1/N$ and the last term denotes the self-energy of each rod. For higher interaction strengths, we obtain the free

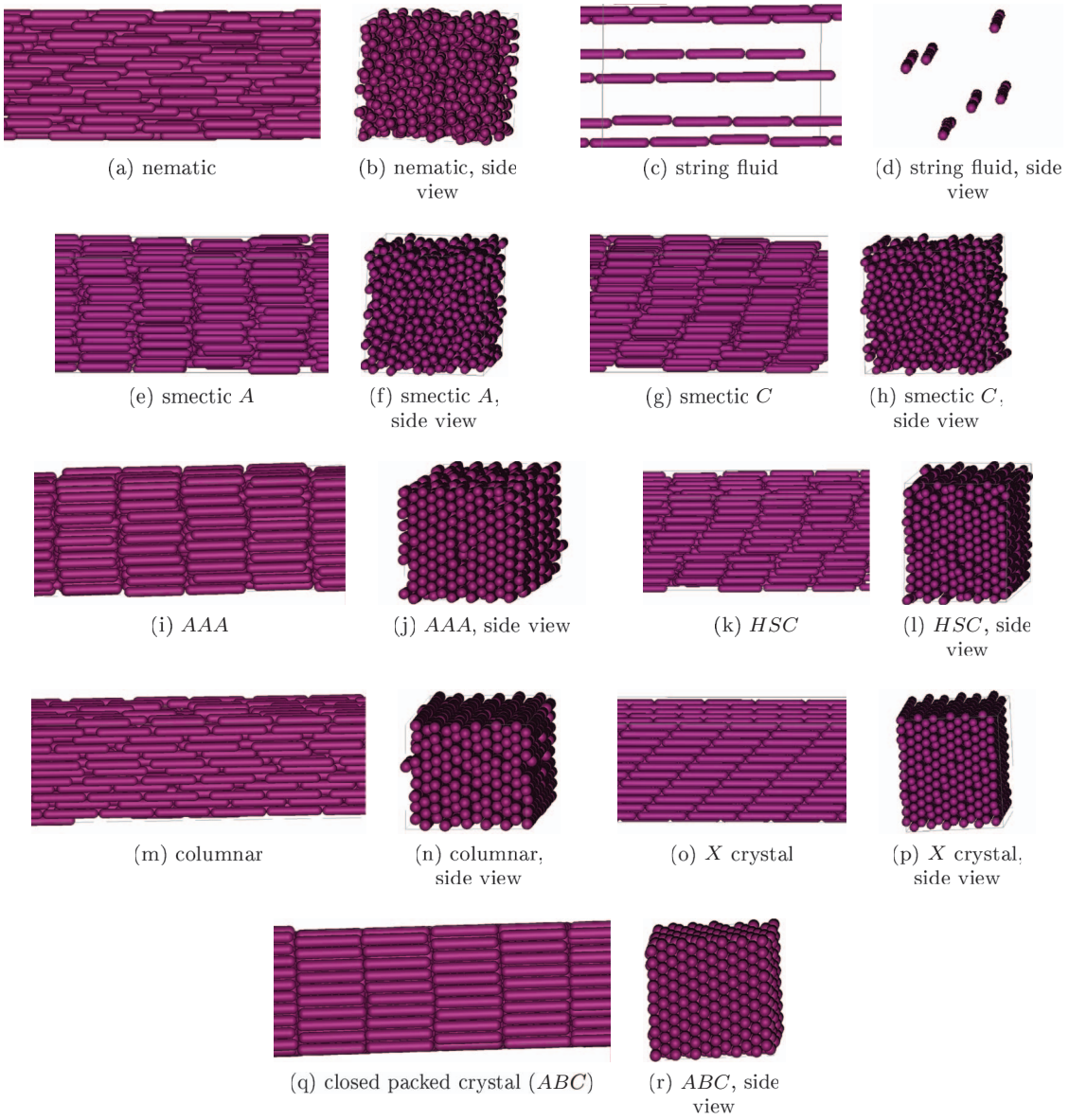

FIG. 4. Typical configuration of the observed phases in a system of $N = 864$ hard parallel spherocylinders with $L/D = 5$ in the double-charge model with $\delta_z = 0.276D$.

energy from the nematic in the zero-field limit by thermodynamic integration. Specifically, if we know the free energy of the nematic at coupling strength γ_1, and if we are able to construct a smooth path to another coupling strength γ_2, then the free energy of the nematic at γ_2 is given by

$$\beta f(\gamma_2) = \beta f(\gamma_1) + \frac{1}{N}\int_{\gamma_1}^{\gamma_2} d\gamma \frac{\langle \beta U \rangle_\gamma}{\gamma}, \tag{12}$$

where N is the number of particles, $\langle \cdot \rangle_\gamma$ denotes an ensemble average taken at interaction strength γ, and

$$\beta U = \frac{1}{2}\sum_{i \neq j} \beta V_{\mathrm{dc}}(\mathbf{r}_i - \mathbf{r}_j) \tag{13}$$

is the pairwise interaction energy due to the polarization of the rods.

2. Free energy of the crystal phases

The free energy of the crystal phase at a fixed density can be obtained through thermodynamic integration from an Einstein crystal. We consider a potential energy function of the form

$$\tilde{U}(\mathbf{r}^N, \lambda) = U(\mathbf{r}_0^N) + \left(1 - \frac{\lambda}{\lambda_{max}}\right)\left[U(\mathbf{r}^N) - U(\mathbf{r}_0^N)\right] + \lambda \sum_{i=1}^{N} \frac{|\mathbf{r}_i - \mathbf{r}_{0,i}|^2}{D^2}, \tag{14}$$

where $\mathbf{r}_{0,i}$ denotes the lattice position of rod i and $U(\mathbf{r}_0^N)$ the corresponding electrostatic energy of the undisturbed crystal as a whole. Note that when $\lambda = 0$ the system interacts purely through electrostatics and the hard cores and for $\lambda = \lambda_{max}$ we recover the Einstein crystal. We can then determine the free

energy of our system by considering[25]

$$\beta f = \beta f^{Ein} + \frac{1}{N}\int_{\lambda=\lambda_{max}}^{\lambda=0} d\lambda \left\langle \frac{\partial \tilde{U}(\mathbf{r}^N,\lambda)}{d\lambda}\right\rangle_\lambda$$
$$= \beta f^{Ein} + \frac{1}{N}\int_{\lambda_{max}}^{0} d\lambda \left\langle \sum_{i=1}^{N} \frac{|\mathbf{r}_i - \mathbf{r}_{0,i}|^2}{D^2} - \frac{U(\mathbf{r}^N) - U(\mathbf{r}_0^N)}{\lambda_{max}}\right\rangle_\lambda . \quad (15)$$

For a d-dimensional system, the free energy of the Einstein crystal plus center of mass corrections is given by[26]

$$\beta f^{Ein} = \frac{\beta U(\mathbf{r}_0^N)}{N} - \frac{d(N-1)}{2}\ln(\pi/\lambda_{max}) + \log \rho\Lambda^3 - \frac{d}{2}\log N. \quad (16)$$

Once the Helmholtz free energy at a specific density ρ_1 is known, we can then use a second thermodynamic integration to calculate the Helmholtz free energy per particle as a function of the density ρ. In particular,

$$\beta f(\rho) = \beta f(\rho_1) + \int_{\rho_1}^{\rho} d\rho' \frac{\beta P(\rho')}{\rho'^2}. \quad (17)$$

3. Free energy of the columnar phase

To calculate the free energy of the columnar phase, we integrate the internal energy from the low temperature X crystal according to Eq. (12). We note that the integration path was smooth and no hysteresis was observed along the integration path.

C. Phase behaviour

To examine the stability of the candidate phases, we performed NPT Monte Carlo simulations of $N = 864$ rods. The simulations were carried out by starting in the ABC, AAA, and X phases at high density with a subsequent expansion of the system at fixed pressure, and in the nematic, smectic A, and string fluid phases with subsequent compression of the system. All simulations were carried out for at least 400 000 MC cycles, half of these for equilibration and the other half for sampling. Changes of the box dimensions were attempted separately for each spatial direction. The equations of state for four representative interaction strengths, e.g., $\gamma = 0$, 0.05, 0.25, and 1, are shown in Fig. 5. The phase diagram in the plane spanned by the interaction strength γ and the packing fraction η, which summarizes all of our results, is shown in Fig. 6. The colored dots indicate points where equation of state calculations were performed. Metastable points and points in the coexistence regions are not plotted. The coexistences were calculated using free energy calculations in combination with common tangent constructions. The thin lines indicate approximate boundaries between phases, such as the smectic A and smectic C phases which will be discussed further below.

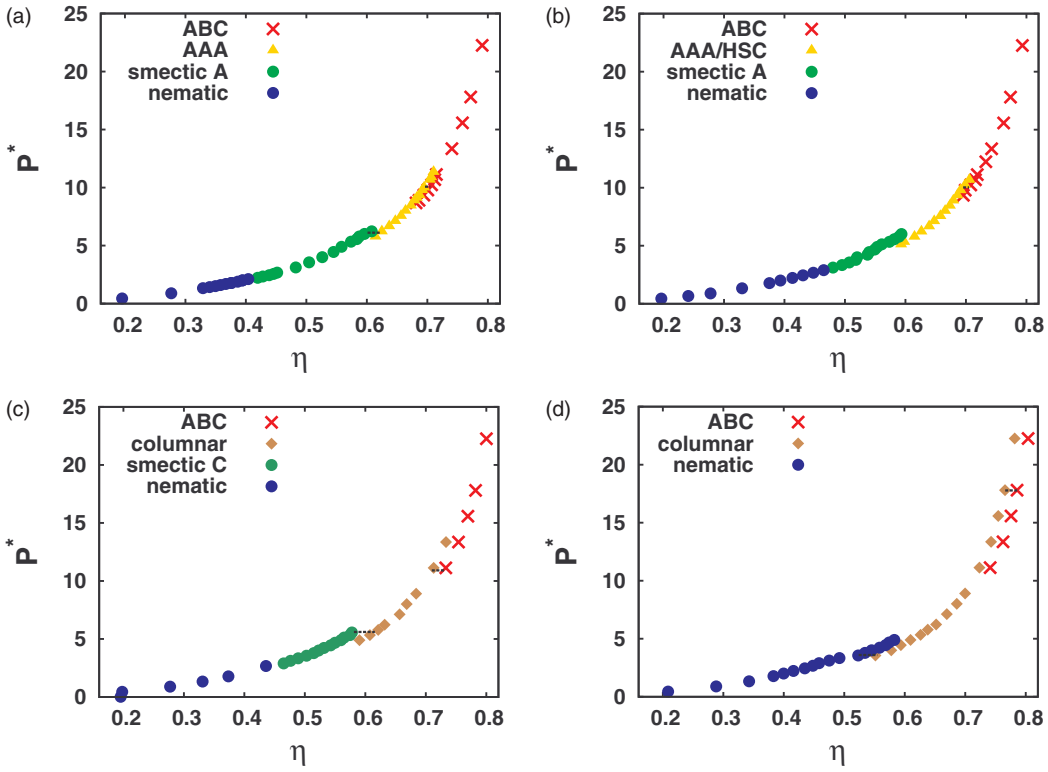

FIG. 5. Equations of state for (a) $\gamma = 0$, e.g., the hard rod case, (b) $\gamma = 0.05$, (c) $\gamma = 0.25$, and (d) $\gamma = 1$, with pressure $P^* = \beta p v_{\text{rod}}$. Different colors indicate different phases as indicated. The distinction between the nematic and smectic phases were made based on visual inspection of simulation snapshots. For the other transitions, the coexistence densities were determined using free energy calculations, and the black dashed lines indicate the two-phase coexistence regions. Note that the equations of state of the nematic, smectic, and AAA crystal associated with $\gamma = 0$ (panel (a)) are consistent with those in Ref. 23.

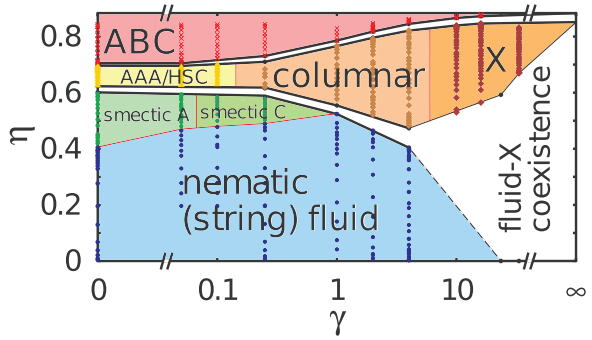

FIG. 6. The phase diagram of a system of $N = 864$ hard, parallel, spherocylinders subject to an external E-field, in the plane spanned by the interaction strength γ and the packing fraction η.

The equations of state and the phase diagram display a variety of stable phases, including a nematic (string) fluid, smectic *A*, and smectic *C* phases, a columnar phase and four crystal phases denoted *AAA*, *HSC*, *X*, and *ABC*. In Secs. III C 1–III C 3, we will discuss a number of these phases individually.

1. String fluid and smectic phases

As seen both in the phase diagram and the equations of state, at low densities and low γ we find a nematic fluid phase. Upon increasing the interaction strength, the rods self-assemble into strings in the direction parallel to the field direction. Interestingly, a similar model studied in Ref. 24, with freely rotating rods of aspect ratio $L/D = 2$ and $\delta_z = 0$ did not exhibit a string phase. For our system, i.e., $L/D = 5$ and with $\delta_z = 0.276D$, the head-to-toe configuration is clearly the energetically most favorable one for two hard parallel spherocylinders, while $\delta_z = 0$ yields only a weakly pronounced minimum at this position. This might explain why Rotunno *et al.*[24] did not observe string formation of spherocylinders, as one would expect on the basis of earlier studies on dipolar spheres.[1,2]

As we increase the density, we find that the nematic (string) fluid transforms via a weakly first order phase transition into a smectic *A* or smectic *C* phase, depending on the interaction strength γ. We observe effectively no hysteresis between the nematic and smectic phases (see Figs. 5(a)–5(c)) and the distinction between these phases is determined via visual inspection of the snapshots in the simulations. As these phase boundaries are based on observations in contrast to free-energy calculations, we denote the boundary between these phases via thin lines in the phase diagram. At interaction strengths larger than $\gamma \approx 1$, the smectic phases disappear completely. Note that the value of γ for which the smectic *A* transforms to a smectic *C* and the one at which the smectic phases disappear altogether are approximate. Their accuracy is determined by the values of γ where we performed equation of state calculations (as indicated by the points in the phase diagram).

At high field strengths, a huge density gap opens up that separates a dilute gaseous state from a dense crystalline *X* state, where we note that we were unable to completely equilibrate the dilute nematic phase. As a result, the coexistence points for high γ ($\gamma > 5$) were determined using the ideal gas free energy of rods and the crystal *X*. We point out here that for high γ the density of the gas coexisting with the crystal approaches zero, and hence the ideal-gas approximation is valid.

2. AAA, HSC, X, and columnar phases

For intermediate densities, with $\gamma = 0$ we find an *AAA* crystal phase in accordance with the hard-rod results of Ref. 23. As the interaction strength is increased, the *AAA* phase begins to compete with the *HSC* phase, and our simulations oscillate between the two phases. We suspect that this is due to finite size effects, but due to computational difficulty we are unable to determine this with certainty. As the interaction strength is further increased to approximately $\gamma \approx 0.2$, the system forms a columnar phase, and finally at $\gamma \approx 10$ the columnar phase is replaced by an *X* crystal. In our phase diagram, we depict the transition between the columnar phase and the *X* crystal phase with a thin line that is approximately half way between the points where each phase is observed. The transition from the nematic and smectic phases at low densities to the columnar and crystalline phases are all first-order, and marked by a clear density jump in the equations of state, as seen in Fig. 5.

We would like to note here that columnar phases are difficult to study in simulations due to finite size effects. In fact, early studies of hard, parallel, spherocylinders identified a columnar phase at intermediate densities instead of the *AAA* as a result of finite size effects.[23] In our simulations (with $N = 864$), in the region where the columnar phase is identified, we only observe a columnar phase, and see spontaneous melting of the *AAA* and *HSC* crystals. However, as the long range nature of the interactions prohibits the study of significantly larger system sizes, we cannot exclude the possibility that some, or all statepoints, of the columnar branch are crystalline in the infinite system limit.

3. ABC phase

At sufficiently high densities, the system always forms an *ABC* crystal as this is the closest packed structure for this system. In the *ABC* crystal phase, the rods are not positioned in head-to-toe configurations, in contrast to the *X*, and columnar phases. As a result, the potential energy of the *ABC* crystal is significantly higher. Thus, the density for which this phase sets in depends highly on the interaction strength, starting around $\eta = 0.7$ for low interaction strength and increasing almost to close packing at high interaction strength. Note that in all cases, this transformation to the *ABC* crystal phase occurs via a first order phase transition, as illustrated by the density jumps in Fig. 5.

D. Experimental comparison

A complete comparison between this phase diagram and experimental observations on colloidal silica rods suspended in a mixture of dimethylsulfoxide (DMSO) and water is

presented in Ref. 19. Using the experimental parameters, we can relate the interaction strength γ to the experimental field strength via $\gamma = 1692.17E^2$, where E is measured in V/μm. Here, we give a short summary.

To start, the main difference between the simulations and the experiments is the presence of an isotropic phase at low field strengths and low densities. This phase cannot occur in our simulations as the rods are explicitly restricted to be parallel. However, at slightly higher field strengths, the isotropic phase turns into a nematic phase similar to what we predict in our phase diagram. The experiments also observe a smectic phase and a single crystalline phase. Importantly, confocal images of cuts through the crystalline phase are consistent with the *X* crystal predicted here, supporting our model. We should remark here that the experiments did not observe a columnar phase, nor *AAA*, *HSC*, *ABC* crystal phases. However, this might simply be a result of the limited number of state points studied experimentally. Specifically, the *ABC* crystal phase is unlikely to be observed in experiments due to the high densities, or equivalently high pressures, needed to access this phase.

IV. CONCLUSION

We have introduced and studied a model system for polarizable spherocylinders of aspect ratio $L/D = 5$ in an external electric field. In our model, we represented the polarizable spherocylinders by parallel spherocylinders with two opposite point charges located near the opposite ends of the rods (Fig. 1), which we called a double charge model. By comparing with a permanent dipole model, we were able to establish a good location for the point charges. By assuming that the rods were a uniformly polarized dielectric we were able to connect the interaction strength of the double charge model to the strength of the applied field assuming the dielectric constants of the rod and the solvent were known.

Using our double charge model, we have predicted the phase diagram for polarizable spherocylinders of aspect ratio $L/D = 5$ in an external electric field. We find regions of stability of a nematic (string) fluid, a columnar phase, two smectic phases, as well as the crystal phases *AAA*, *HSC*, *X*, and *ABC*. Our results at zero field, i.e., zero interaction strength, agreed well with previous simulations studies. In an additional study, we demonstrate that our results show good qualitative agreement with experiments on colloidal silica rods in an external electric field.[19]

ACKNOWLEDGMENTS

This work is part of the D-ITP consortium and part of the DFG/FOM program SFB-TR6 (project B8), programs of the Netherlands Organisation for Scientific Research (NWO) that is funded by the Dutch Ministry of Education, Culture and Science (OCW). L.F. would also like to acknowledge funding from the Sectorplan Natuur- en Scheikunde (Netherlands).

[1] A. P. Hynninen and M. Dijkstra, Phys. Rev. E **72**, 051402 (2005).
[2] A. P. Hynninen and M. Dijkstra, Phys. Rev. Lett. **94**, 138303 (2005).
[3] A. Yethiraj and A. van Blaaderen, Nature **421**, 513 (2003).
[4] L. Rossi, S. Sacanna, and K. P. Velikov, Soft Matter **7**, 64 (2010).
[5] A. Kuijk, A. van Blaaderen, and A. Imhof, J. Am. Chem. Soc. **133**, 2346 (2011).
[6] A. Kuijk, D. V. Byelov, A. V. Pethukov, A. van Blaaderen, and A. Imhof, Faraday Discuss. **159**, 181 (2012).
[7] D. Nagao, M. Sugimoto, A. Okada, H. Ishii, M. Konno, A. Imhof, and A. van Blaaderen, Langmuir **28**, 6546 (2012).
[8] A. F. Demirörs, P. M. Johnson, C. M. van Kats, A. van Blaaderen, and A. Imhof, Langmuir **26**, 14466 (2010).
[9] P. M. Johnson, C. M. van Kats, and A. van Blaaderen, Langmuir **21**, 11510 (2005).
[10] D. Nagao, M. Hashimoto, K. Hayasaka, and M. Konno, Macromol. Rapid Commun. **29**, 1484 (2008).
[11] B. Peng, H. R. Vutukuri, A. van Blaaderen, and A. Imhof, J. Mater. Chem. **22**, 21893 (2012).
[12] M. Marechal, R. J. Kortschot, A. F. Demirörs, A. Imhof, and M. Dijkstra, Nano Lett. **10**, 1907 (2010).
[13] C. I. Zoldesi, C. A. van Walree, and A. Imhof, Langmuir **22**, 4343 (2006).
[14] S. Sacanna and D. J. Pine, Curr. Opin. Colloid Interface Sci. **16**, 96 (2011).
[15] M. Mittal and E. M. Furst, Adv. Funct. Mater. **19**, 3271 (2009).
[16] B. W. Kwaadgras, M. Verdult, M. Dijkstra, and R. van Roij, J. Chem. Phys. **135**, 134105 (2011).
[17] T. Troppenz, A. Kuijk, A. Imhof, A. van Blaaderen, M. Dijkstra, and R. van Roij, "Nematic ordering of polarizable colloidal rods in an external electric field: theory and experiment" (unpublished).
[18] J. P. Singh, P. P. Lele, F. Nettesheim, N. J. Wagner, and E. M. Furst, Phys. Rev. E **79**, 050401 (2009).
[19] A. Kuijk, T. Troppenz, L. Filion, A. Imhof, R. van Roij, M. Dijkstra, and A. van Blaaderen, Soft Matter **10**, 6249 (2014).
[20] S. C. McGrother, D. C. Williamson, and G. Jackson, J. Chem. Phys. **104**, 6755 (1996).
[21] In a typical experimental, colloidal system, α is fairly small and the electric field resulting from the induced dipole moments is much weaker than the applied the external field strength. In particular, for the system discussed at the end of this paper, the field of a rod, as calculated at the center of a neighbouring rod via the double charge model, is less than 2% of the external field strength.
[22] See supplementary material at http://dx.doi.org/10.1063/1.4897562 for further information.
[23] J. A. C. Veerman and D. Frenkel, Phys. Rev. A **43**, 4334 (1991).
[24] M. Rotunno, T. Bellini, Y. Lansac, and M. A. Glaser, J. Chem. Phys. **121**, 5541 (2004).
[25] D. Frenkel and B. Smit, *Understanding Molecular Simulations: From Algorithms to Applications* (Academic Press, 2002).
[26] J. M. Polson, E. Trizac, S. Pronk, and D. Frenkel, J. Chem. Phys. **112**, 5339 (2000).